Faraday Discussions

Accepted Manuscript

This manuscript will be presented and discussed at a forthcoming Faraday Discussion meeting. All delegates can contribute to the discussion which will be included in the final volume.

Register now to attend! Full details of all upcoming meetings: http://rsc.li/fd-upcoming-meetings

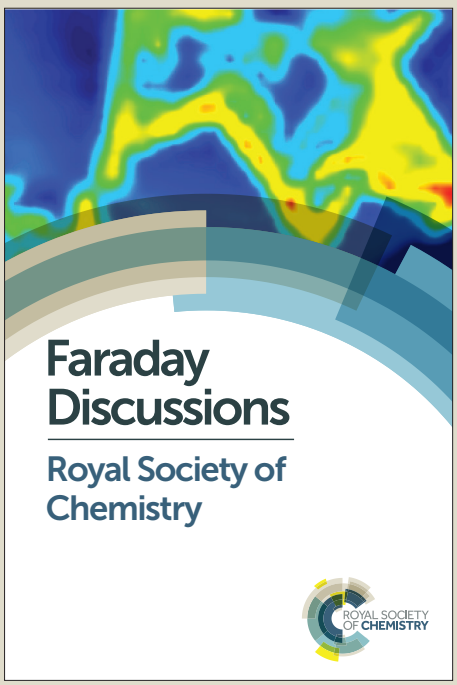

This is an *Accepted Manuscript*, which has been through the Royal Society of Chemistry peer review process and has been accepted for publication.

Accepted Manuscripts are published online shortly after acceptance, before technical editing, formatting and proof reading. Using this free service, authors can make their results available to the community, in citable form, before we publish the edited article. We will replace this *Accepted Manuscript* with the edited and formatted *Advance Article* as soon as it is available.

You can find more information about *Accepted Manuscripts* in the Information for Authors.

Please note that technical editing may introduce minor changes to the text and/or graphics, which may alter content. The journal's standard Terms & Conditions and the Ethical guidelines still apply. In no event shall the Royal Society of Chemistry be held responsible for any errors or omissions in this *Accepted Manuscript* or any consequences arising from the use of any information it contains.

ROYAL SOCIETY OF CHEMISTRY

www.rsc.org/faraday_d

Using degrees of rate control to improve selective n-butane oxidation over model MOF-encapsulated catalysts: sterically-constrained $Ag_3Pd(111)$

Sean T. Dix[a], Joseph K. Scott[a], Rachel B. Getman[a] and Charles T. Campbell*[b]*

[a] Department of Chemical and Biomolecular Engineering, Clemson University, Clemson, SC 29634, USA
[b] Department of Chemistry, University of Washington, Seattle, WA 98195-1700, USA
*corresponding authors' emails: rgetman@clemson.edu and charliec@uw.edu

Abstract

Metal nanoparticles encapsulated within metal organic frameworks (MOFs) offer steric restrictions near the catalytic metal that can improve selectivity, much like in enzymes. A microkinetic model is developed for the regio-selective oxidation of n-butane to 1-butanol with O_2 over a model for MOF-encapsulated bimetallic nanoparticles. The model consists of a $Ag_3Pd(111)$ surface decorated with a 2-atom-thick ring of (immobile) helium atoms which creates an artificial pore of similar size to that in common MOFs, which sterically constrains the adsorbed reaction intermediates. The kinetic parameters are based on energies calculated previously using density functional theory (DFT). Activation of the C-H bond is assisted by oxygen adatoms, leading to 1-butanol and butanal products. The model was analysed to determine which species (adsorbed intermediates and transition states in the reaction mechanism) have energies that most sensitively affect the reaction rates to the different products, using degree-of-rate-control (DRC) analysis. This DRC analysis revealed that the production of the adsorbed OH needed to make butanol was mainly via the dehydrogenation of butoxy to make butanal plus OH, thus limiting selectivity to near 50%. This suggested that water should be added to the feed to make more OH, which indeed increased the rate to butanol and its selectivity to 70%. Moreover, ~15% less O_2 was consumed per oxygen atom in the products. The degree of rate control for the oxidation adsorbed butane to butoxy plus H was positive for making butanol but negative for making butanal, suggesting that an increase in butane pressure should improve selectivity. This indeed increased the selectivity to 100%, the rate to butanol increased slightly, and O_2 was now used to make only ~50% of the oxygen atom in the products.

Keywords: alcohol, C-H bond activation, oxidation, oxygen activation, regioselectivity

Faraday Discussions Accepted Manuscript

1. Introduction

The steric environmental surrounding the metal site in metallo-enzymes is often thought to impart selectivity in its catalytic products. It has been shown that this same type of effect can be achieved in synthetic catalyst structures where catalytic nanoparticles (NPs) are encapsulated by metal-organic frameworks (MOFs), known as NP@MOF systems.[1-5] For example, Stephenson *et al.*[5] achieved 95% selectivity in the hydrogenation of 1,3-hexene to 3-hexene by encapsulating ~3 nm Pt particles in the MOF ZIF-8. Without ZIF-8, n-hexane is formed instead with 80% selectivity.

With the goal of using DFT calculations to help develop NP@MOF catalysts, but aiming to circumvent the unknown details of the NP/MOF interface, Gomez-Gualdron *et al.*[6] introduced a simplified approach where steric constraints near the catalyst surface are provided by a "surrogate" pore formed by chemically inert atoms. They showed that this steric constraint on a Pd catalyst may facilitate the C-H activation of n-butane due to the different relative destabilization of n-butane and 1-butyl, relevant to selective oxidation of n-butane to 1-butanol.

In a previous study, we used this "surrogate pore" approach together with DFT to investigate whether this steric constraint is sufficient to achieve regio-selective oxidation of n-butane to 1-butanol on Ag_3Pd bimetallic nanoparticles. Specifically, we studied the (111) facet of a Ag_3Pd alloy, where the MOF-mimetic pore is modelled by two rings of 9 He atoms each, stacked on top of each other and frozen in space in the geometry shown on the left in Fig. 1.[6] A butanol molecule is included in the right of Fig. 1 to demonstrate that only its terminal C atoms have access to the metal atoms in this catalyst, due to steric constraints imposed by the (frozen) He_{18} ring. This allowed oxygen addition only to the terminal carbons.

Faraday Discussions Accepted Manuscript

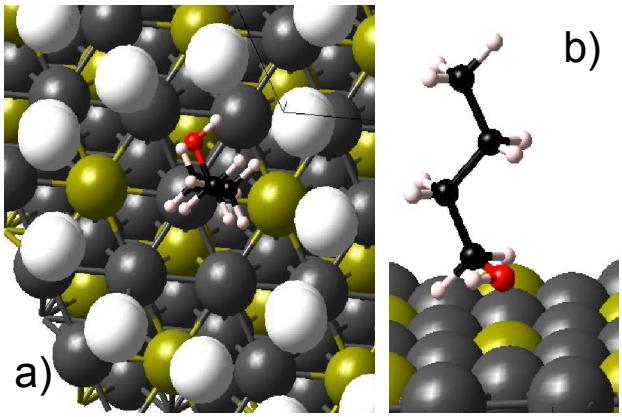

Figure 1. a) Top view of adsorbed n-butanol on the He ring-encapsulated $Ag_3Pd(111)$ surface. b) Side view of the same system shown in panel *a* but with the He atoms removed to view the surface sites better. Ag = grey, Pd = yellow, C = black, H = off-white, O = red, He rings = white.

We use that same model here to develop a microkinetic model to predict the reaction rates to the various potential products at a specific set of reaction conditions chosen to approximately simulate experimental conditions for gas phase butane oxidation. The energies of its adsorbed intermediates and transition states were taken from the DFT calculations reported in that previous study.[7] We also analyse this new microkinetic model to determine the degree of rate control (DRC) of every elementary step's transition state and every adsorbed intermediate, with respect to the rate of production of every possible product and the rate of consumption of the most expensive reactant, butane. The DRCs (X_i) of each adsorbed intermediate and transition state for every elementary step are defined as outlined in Ref. [8]:

$$X_i = \left(\frac{\partial \ln r}{\partial \left(\frac{-G_i^0}{RT} \right)} \right)_{G_{j \neq i}^0} \qquad \text{Equation 1}$$

where r is the net rate of formation of one product (e.g., butanol, butanal, or 1-butene oxide gas), or the net rate of consumption of one reactant (e.g., butane), G_i^0 is the standard-state free energy of species i (e.g., one adsorbed intermediate or transition state), R is the gas constant, and T is the absolute temperature. In practice, these partial derivatives are calculated numerically, with the change in G_i^0 easily implemented by simply changing the electronic energy of species i by a tiny amount from the value actually calculated by DFT. The DRC values are nearly zero for most species, but by finding the species with large values, we are able to define which species' energies need to be tuned in what directions by further material modifications in order to achieve a more effective catalyst in terms of activity and selectivity, which should be useful in supplying

Faraday Discussions Accepted Manuscript

ideas for catalyst optimization. A fast computational method for using such DRC values from such a reference catalyst as studied here to search for better catalyst materials has recently been developed.[9] We have discovered here through this DRC analysis how to tune the reactant feed to achieve much better selectivity to butanol (100%) and a faster rate with much less consumption of O_2.

2. Methods

We study selective butane oxidation, with butanol as the desired product, over a MOF-encapsulated $Ag_3Pd(111)$ catalyst model, initially with O_2 as the only oxidant, at 0.64 bar total pressure and temperature of 373 K. The $Ag_3Pd(111)$ catalyst surface was modelled by cutting a 4-layer, 4 metal atom × 4 metal atom (111) surface from the bulk $L1_2$ structure of Ag_3Pd. Steric constraints imposed by the MOF are provided by the surrogate pore approach, which has been introduced, described, and validated in detail by Gomez-Gualdron *et al*.[6] The surrogate pore limits the way C_4 species can interact with catalyst surface, while imparting only weak dispersion interactions. It is composed of chemically inert helium atoms (Figure 1), the positions of which remain fixed during the simulations. The helium atoms form two rings, each composed of nine helium atoms.

The reaction network is initially comprised of 17 reactions, each in forward and reverse, including the desired formation of 1-butanol and competing undesired formation of 1-butanal and 1-butene oxide, which represent the first steps in over-dehydrogenation of the primary and secondary carbons, respectively.[7] The elementary steps are listed in Table 1 along with each step's reaction energy and activation energy in the forward direction as written, obtained from density functional theory (DFT) calculations reported in a prior publication.[7] Our analysis in this work indicates that the coverages of all intermediates are low (i.e., less than 0.25 ML) during the catalysis, hence all values are reported at such coverages. The exceptions are the coverage of n-butane and 1-butanol, which exceed 0.25 ML under some of the conditions reported; however, as we previously reported,[7] these adsorbates exhibit only weak neighbour interactions, so we do not expect higher coverages of them to influence the reaction energies and activation barriers used here. Reaction energies and activation barriers for reactions 3, 11, and 14-17 were either not previously reported, or they were not reported at low coverage, and thus their values in Table 1 are being reported first here. Additionally, some of the values reported in previous work used

Faraday Discussions Accepted Manuscript

configurations of adsorbates that exhibited significant first-nearest-neighbour interactions, and these contributions have been removed from the energies used for this work by adding/subtracting the appropriate quantities from those adsorbate and transition state energies. The first-nearest-neighbour interaction energies used for this were reported in a prior publication.[7] Additionally, for this publication, we calculated the first-nearest-neighbor interaction energies between two hydroxyls, i.e., OH*-OH*, to be 0.13 eV, and between a surface water molecule and O*, i.e., H_2O*-O*, to be -0.25 eV. DFT calculations were performed with the VASP code,[10, 11] which utilizes periodic boundary conditions and plane wave basis sets. Valence electron exchange and correlation were calculated with the PBE functional,[12, 13] while core electrons were simulated with PAW pseudopotentials[14, 15] to an energy cut-off of 400 eV. The D2 method of Grimme[16] was employed in all calculations to improve the modelling of dispersion interactions. Gamma-centred **k**-point meshes of 7×7×1 were used to sample the first Brillouin zones. Transition states (TSs) were located with a combination of the Climbing Image Nudged Elastic Band (CI-NEB)[17, 18] and dimer methods.[19] Other details of the DFT calculations are given in Ref. [7].

Table 1. Elementary reaction steps considered in the microkinetic model and the DFT-derived reaction energy and activation barrier for each, in units of eV. The * refers to a metal surface site. From Ref. [7].

Rxn #	Reaction	ΔE_{rxn}	ΔE_{act}
1	$O_2 + * = O_2*$	−0.52	0
2	$O_2* + * = 2O*$	−1.05	0.66
3	$O_2* + C_4H_{10}* = C_4H_9OH* + O*$	−2.86	1.12
4	$C_4H_{10}* + O* = C_4H_9O* + H*$	−0.03	0.35
5	$C_4H_{10}* + O* = C_4H_9* + OH*$	−0.12	1.19
6	$C_4H_{10}* + O* = C_4H_9OH* + *$	−1.10	1.22
7	$C_4H_9O* + O* = C_4H_8Oep* + OH*$	−0.17	0.94
8	$C_4H_9O* + O* = C_4H_8Oal* + OH*$	−0.85	0.39
9	$C_4H_9O* + H* = C_4H_9OH* + *$	−0.76	0.43
10	$C_4H_9* + OH* = C_4H_9OH* + *$	−1.36	0.76
11	$C_4H_9O* + OH* = C_4H_9OH* + O*$	+0.05	0.14
12	$C_4H_{10} + * = C_4H_{10}*$	−0.47	0
13	$C_4H_9OH* = C_4H_9OH + *$	+0.79	0.79
14[a]	$C_4H_8Oal* = C_4H_8Oal + *$	+0.70	0.70
15[b]	$C_4H_8Oep* = C_4H_8Oep + *$	+0.49	0.49
16	$2H* = H_2\ (g) + 2*$	+0.20	0.20
17	$O* + H* = OH* + *$	−1.50	0.72

[a] "al" means 1-butanal [b] "ep" means 1-butene oxide

Faraday Discussions Accepted Manuscript

We supplied the temperature and inlet flow rates of all reactants and products, and solved for the steady state concentrations in the limits of low (differentional) further conversion using all 17 reactions presented below in the equation solver. The equation solver was the ode15s function as implemented in MATLAB.

We model here a differential CSTR (continuous stirred tank reactor), where the percent change in partial pressures (effectively also representing the inlet to outlet of a differential length element in a well-mixed flow reactor) is < 1% of the inlet partial pressure for all species. To track the rates of butane adsorption, butanol desorption, and butanal desorption, we used units of moles/second for the rates. This way, the rates to products can be directly compared with the rates of the surface reactions. To obtain the rates of the surface reactions, we assumed a value for the number of catalyst sites per reactor volume of 1.1×10^{25} sites/m^3.

The degrees of rate control of each adsorbed intermediate and the transition state for every elementary step were determined numerically using the definition of the DRC,[8] except for those reaction steps that have no real barrier (i.e., where the potential energy only drops from reactant to products). In those cases, it is impossible to incrementally decrease the energy of the transition state, as required by that exact definition, without also decreasing that for the reactant. For such "downhill-only" steps, we instead incrementally increased the transition state energy (to be slightly larger than the reactant), and changed the sign on the resulting change in rate needed in the definition of this transition state's DRC. This gives a value for the DRC that has the same essential meaning as intended by the original definition in Ref. [8], but broadens the applicability to such usual steps (i.e., "downhill only"). The absolute magnitude of all incremental energy changes used to calculate DRCs was 10^{-8} eV.

3. Results

3.1. Original mechanism

We studied the reaction kinetics under steady-state, differential conversion conditions, at T = 373 K and inlet partial pressures of 21.3 kPa O_2 (g), 42.6 kPa C_4H_{10} (g), 0.010 kPa C_4H_9OH (g), 0.010 kPa C_4H_8O (al, g), and 0.010 kPa H_2 (g). Here, "al" indicates that the C_4H_8O species is 1-butanal, and not 1-butene oxide. These conditions are meant to represent a differential length element very early in a flow reactor, but far enough along that we can calculate steady-state

Faraday Discussions Accepted Manuscript

differential conversions with small percentage changes in all concentrations. The TOF to butanol was found to be 3.2×10^{5} molecule site^{-1} s^{-1}, with a selectivity, defined as the amount of 1-butanol formed divided by amount of butane reacted, of 58%. The only other significant products were 1-butanal, at 42% selectivity, and consequently, H_2(g). The differential increase in conversion of butane was 0.13%. Table 2 shows the corresponding steady-state coverages of adsorbed intermediates at these conditions. The most abundant surface intermediate is 1-BuOH, with a coverage of ~ 0.25 ML. Other adsorbed intermediates with non-tiny coverages are O_2 (0.1 ML) and OH (0.06 ML). About 55% of the sites are unoccupied.

Table 2. Steady-state coverages of surface intermediates using the reactions listed in Table 1, under reaction conditions of: T = 373 K and inlet partial pressures of 21.3 kPa O_2 (g), 42.6 kPa C_4H_{10} (g), 0.010 kPa C_4H_9OH (g), 0.010 kPa C_4H_8O (al, g), and 0.010 kPa H_2 (g).

Intermediate	θ (ML)
O*	7.16×10^{-4}
O_2*	0.0974
C_4H_{10}*	0.0168
C_4H_9*	3.06×10^{-10}
OH*	0.0611
C_4H_9O*	0.0140
H*	9.44×10^{-4}
C_4H_8Oep*[a]	4.79×10^{-13}
C_4H_8Oal*[b]	0.0126
C_4H_9OH*	0.252
*	0.545

[a] "al" means 1-butanal
[b] "ep" means 1-butene oxide

The corresponding DRCs for all adsorbates are shown in Table 3. As expected, these DRCs of adsorbed intermediates are approximately proportional to their coverages in Table 2, with the proportionality constant being negative[8] (-1.3 in this case). Small differences may be associated with errors that are due to code-related computer accuracy. This shows that the usual situation occurs here: When adsorbed intermediates that have significant coverages are stabilized in energy, their coverages increase and this poisons the rate controlling step(s).[8]

Faraday Discussions Accepted Manuscript

Table 3. DRCs of the adsorbed intermediates for the same reactions and conditions as Table 2.

Intermediate	$X_{butanol}$	$X_{butanal}$	$X_{butene\ oxide}$	X_{butane}
O*	-0.00170	-0.00159	-0.00159	-0.00166
O_2*	-0.131	-0.123	-0.123	-0.128
C_4H_{10}*	-0.0234	-0.0218	-0.0218	-0.0227
C_4H_9*	0	0	0	0
OH*	-0.0834	-0.0779	-0.0779	-0.0811
C_4H_9O*	-0.0188	-0.0175	-0.0175	-0.0183
H*	-0.00603	-0.00563	-0.00563	-0.00589
C_4H_8Oep*[a]	-0.00131	-0.00122	-0.00122	-0.00113
C_4H_8Oal*[b]	-0.0161	-0.0151	-0.0151	-0.0157
C_4H_9OH*	-0.340	-0.318	-0.318	-0.331

[a] "al" means 1-butanal

[b] "ep" means 1-butene oxide

Table 4 shows the corresponding DRCs for all the transition states (i.e., for each elementary step). Also shown are the net steady-state reaction rates for each step, and the ratio of the forward rate for that step to its net rate. For most steps, this ratio is 1.0, which means the step proceeds only in the forward direction. For all the other steps (except step (4)) it is huge (>46), meaning that the step is fast to equilibrium. The ratio for step (4) is near 2, indicating an intermediate case.

Faraday Discussions Accepted Manuscript

Table 4. Steady-state turnover frequencies (TOFs), ratio of forward TOF to net TOF, and degrees of rate control (X) for each elementary step obtained by solving the microkinetic model using the same reactions and conditions as Table 2.

Rxn #	TOF (molecule site^{-1} s^{-1})	Forward TOF/ Net TOF	$X_{butanol}$	$X_{butanal}$	$X_{butene\ oxide}$	X_{butane}
1	27262	5.09×10^{4}	-2.99×10^{-3}	-2.79×10^{-3}	-2.79×10^{-3}	-2.89×10^{-3}
2	27262	1.00	0.572	0.723	0.723	0.636
3	5.14×10^{-4}	1.00	3.52×10^{-4}	3.28×10^{-4}	3.29×10^{-4}	3.37×10^{-4}
4	54525	1.76	0.0885	-0.0248	-0.0248	0.0409
5	4.28×10^{-7}	1.00	-1.23×10^{-5}	-1.14×10^{-5}	-1.14×10^{-5}	-2.40×10^{-5}
6	1.68×10^{-7}	1.00	-2.86×10^{-3}	-2.67×10^{-3}	-2.67×10^{-3}	-2.79×10^{-3}
7	8.48×10^{-4}	1.00	-2.56×10^{-3}	-2.39×10^{-3}	0.998	-2.45×10^{-3}
8	22912	1.00	-0.0774	0.116	-0.884	3.99×10^{-3}
9	8702	1.00	0.0791	-0.196	-0.196	-0.0365
10	4.28×10^{-7}	1.00	0	0	0	0
11	22912	2.04×10^{5}	7.42×10^{-3}	6.93×10^{-3}	6.93×10^{-3}	7.17×10^{-3}
12	54525	3.78×10^{4}	-1.11×10^{-3}	-1.04×10^{-3}	-1.04×10^{-3}	-1.08×10^{-3}
13	31613	59.1	7.23×10^{-3}	6.75×10^{-3}	6.75×10^{-3}	6.97×10^{-3}
14	22912	65.1	-1.00×10^{-3}	-9.38×10^{-4}	-9.38×10^{-4}	-1.01×10^{-3}
15	8.48×10^{-4}	46.1	-1.76×10^{-3}	-1.64×10^{-3}	-1.64×10^{-3}	-1.68×10^{-3}
16	22912	210	-1.34×10^{-3}	-8.01×10^{-4}	-8.01×10^{-4}	-1.13×10^{-3}
17	5.05×10^{-2}	1.00	5.87×10^{-4}	5.47×10^{-4}	5.47×10^{-4}	5.29×10^{-4}

The DRC in the butane consumption rate is large for step 2, and tiny for all other steps. This shows that step (2), $O_2^* + * \rightarrow 2O^*$, is the most rate controlling step (MRCS) in butane consumption. As seen from the DRCs of the adsorbed intermediates, this step is slow due to its large activation barrier, and to some extent because adsorbed butanol is plugging up the free site needed for it to occur. The same is true for DRCs in the rates of production of both 1-BuOH and 1-butanal: Step (2) is the MRCS in the rates to the main products.

However, in the rate of production of 1-butene oxide, two other steps have large DRCs: Step (7) has a DRC of 1.0 and step (8) has a DRC of -0.9. This is because both these steps compete for the same reactants, $C_4H_9O^*$ and O*. Step (7) and (8) reflect a true branching competition, whereby butoxy plus O* selects two different options for how to proceed: making 1-butene oxide vs making 1-butanal (plus OH*, which leads directly to butanol, see below). The DRC to 1-butene oxide for step (7) is +1 but for step (8) it is nearly -1. That is because reaction (8) steals butoxy + O* from reaction (7) every time it occurs. The DRC to 1-BuOH for step (7) is negative, but small in magnitude since only a tiny fraction of the butoxy + O* is consumed via

Faraday Discussions Accepted Manuscript

step (7) (almost all goes via step (8)), so increasing its rate has only a weak impact on the rate of step (8).

Two crucial reactions are steps (8) and (11):

(8) $C_4H_9O^* + O^* = C_4H_8Oal^* + OH^*$ and

(11) $C_4H_9O^* + OH^* = C_4H_9OH^* + O^*$.

At first view, one might guess that these two steps should undergo a similar branching competition, whereby butoxy selects two different options for how to proceed: making 1-butanal vs 1-butanol. But the rate constants are such that step (11) happens once immediately every time reaction (8) occurs once. This is because step (11) is very fast when there is any OH* around, and step (8) is the only kinetically viable path to produce the OH* needed to allow step (11) to go. We initially expected that step (17) (i.e., $O^* + H^* \rightarrow OH^* + *$) would also make OH*, but since the DRC of this step in making 1-butanol is negligible, it clearly makes a negligible contribution. As a consequence, steps (8) and (11) do NOT reflect a true branching competition, but instead two sequential reactions (if considered from the perspective of the OH*, not the butoxy*). This explains why the selectivity to 1-BuOH and 1-butanal are nearly equal to each other at 58% and 42%, respectively: Every 1-butanal produced leads to one OH*, which in turn leads quickly to one 1-BuOH product molecule. The selectivities to each would be exactly 50%, except that there is another route to make 1-BuOH, albeit at a much slower rate: step (9), the protonation of butoxy by H*, which increases its selectivity to 58%.

Looking at the rates and DRCs of all the steps and neglecting the minor pathways, we concluded that the reaction mainly proceeds by the following simplified pathway:

(1)	$O_2 + * = O_2^*$	$\Delta E_{act} = 0$ eV
(2)	$O_2^* + * = 2O^*$	$\Delta E_{act} = 0.66$ eV
(4)	$C_4H_{10}^* + O^* = C_4H_9O^* + H^*$	$\Delta E_{act} = 0.35$ eV
(8)	$C_4H_9O^* + O^* = C_4H_8Oal^* + OH^*$	$\Delta E_{act} = 0.39$ eV
(9)	$C_4H_9O^* + H^* = C_4H_9OH^* + *$	$\Delta E_{act} = 0.43$
(11)	$C_4H_9O^* + OH^* = C_4H_9OH^* + O^*$	$\Delta E_{act} = 0.14$ eV
(12)	$C_4H_{10} + * = C_4H_{10}^*$	$\Delta E_{act} = 0$ eV
(13)	$C_4H_9OH^* = C_4H_9OH + *$	$\Delta E_{act} = 0.79$ eV
(14)	$C_4H_8Oal^* = C_4H_8Oal + *$	$\Delta E_{act} = 0.70$ eV
(16)	$2H^* = H_2\,(g) + 2^*$	$\Delta E_{act} = 0.24$ eV

Faraday Discussions Accepted Manuscript

In other words, O_2 adsorbs rapidly and occasionally dissociates on the surface in the MRCS to make 2 O*. A terminal C-H bond in adsorbed butane is activated by surface O*, forming C_4H_9O* (butoxy) and H*. The C_4H_9O* can react with another surface O* to form C_4H_8Oal* (1-butanal) plus OH*, or it can react with surface OH* (created by that last step), to form C_4H_9OH* (1-butanol). The latter is very stable, so it plugs up the surface sites. The H* produced in step (4) desorbs mainly as H_2, although some is used to protonate butoxy via step (9).

3.2. Including $H_2O + O^* \rightarrow 2\ OH^*$ in the mechanism

It is clear from the above analysis that the one way to get higher selectivity to 1-BuOH over 1-butanal would be to reduce the activation barrier for step (9), $C_4H_9O^* + H^* = C_4H_9OH^* + *$, so that it competes more effectively with step (16) for the H* produced in step (4), perhaps by by destabilizing the C_4H_9O* reactant with a less oxophilic catalyst. Another option would be to find another way to get OH* than via steps (8) and (17). One possibility would be to find a modification that dramatically decreased the activation energy for step (17), $O^* + H^* \rightarrow OH^*$ so it would contribute more to the rate. However, the DRC for this step is so low (6×10^{-4}), it would take a major change it this energy to have much effect. This led us to consider an easier approach: to simply supply some water in the reaction feed, in hopes that it would produce OH* via $H_2O + O^* \rightarrow 2\ OH^*$. This reaction is known to proceed rapidly below room temperature on both Ag and Pt surfaces,[20, 21] although the OH* product of this reaction is often stabilized by adsorption of more water to make a coadsorbed H_2O-OH 1:1 stoichiometric complex.[21] In order to incorporate this reaction in the mechanism, we calculated the energetics of this two-step, oxygen-assisted H_2O dissociation on the $Ag_3Pd(111)$ surface. They are given in Table 5.

Table 5. Additional elementary reaction steps added to the microkinetic model and the DFT-derived reaction energy and activation barrier for each, in units of eV.

Rxn #	Reaction	ΔE_{rxn}	ΔE_{act}
18	$H_2O + * = H_2O^*$	−0.44	0
19	$H_2O^* + O^* = 2OH^*$	−0.15	0.12

Table 6 gives the rates and DRCs for the scenario where these two new reactions are included in the mechanism and a very small amount of H_2O (1.5 kPa) is included in the reactor feed. This decreases the rate of 1-BuOH production, since these new steps provide a way for OH* to escape from the surface, as water. This also untangles step (11) from step (8), since the

Faraday Discussions Accepted Manuscript

production of one OH* in step (8) no longer leads to its consumption via step (11). The OH* now has another kinetically viable route to leave the surface: via the reverse of step (19) followed by step (18) in reverse, thus eliminating two OH*s per H_2O product. This slows down step (11) so much that it is no longer the dominant path to 1-BuOH*, and indeed it goes now so fast in reverse that it consumes most of the 1-BuOH* as it is produced. Step (9) now dominates production of 1-BuOH*, but it is now in direct competition for the same butoxy used in step (8) to make butanal. The net production of butanal is now ~40-fold faster than 1-BuOH, so the DRC to 1-BuOH for step (8) is large and negative (~-4), since every increase in its rate decreases the rate to 1-BuOH by ~40 times that same amount. (i.e., The DRC to butanol for step (8) is roughly this factor of 40 times its DRC to butanal.). For a similar reason, there is a large negative DRC to 1-BuOH for step (2) of -1, since step (2) produces the O* reactant needed in step (8), which in turn robs the butoxy needed to make 1-BuOH*. Similarly, there is a large positive DRC to 1-BuOH for step (4) of +3, since this step produces both the C_4H_9O* and the H* needed to make 1-BuOH* in step (9) in this competition with step (8) to butanal, and, more importantly, it consumes the O* that drives step (11) so fast in the reverse direction to destroy most of the 1-BuOH* just produced. The net effect of adding steps (18) and (19) but very little water is to dramatically decrease the selectivity to butanol to 2.2%. The surface coverage is relatively low at these conditions.

Faraday Discussions Accepted Manuscript

Table 6. Steady state turnover frequencies (TOFs), ratio of forward TOF to net TOF, and degrees of rate control (X) for all elementary steps obtained by solving the microkinetic model using the reactions listed in both Tables 1 and 5. In this case, a low amount amount of H_2O (1.5 kPa) was included in the feed, otherwise the reaction conditions were the same as Tables 2-4.

Rxn #	TOF (molecule site^{-1} s^{-1})	Forward TOF/ Net TOF	$X_{butanol}$	$X_{butanal}$	$X_{butene\ oxide}$	X_{butane}
1	44845	3.98×10^{4}	0.00508	-0.00451	-0.00451	-0.00424
2	44845	1.00	-0.971	1.01	1.01	0.964
3	8.40×10^{-4}	1.00	0.00343	-0.00305	-0.00305	-0.00290
4	53755	2.71	3.00	-0.0993	-0.0993	-0.0311
5	6.51×10^{-7}	1.00	0.00583	-0.00518	-0.00518	-0.00490
6	2.56×10^{-7}	1.00	0	0	0	0
7	1.95×10^{-3}	1.00	-0.00302	0.00268	1.00	0.00246
8	52570	1.00	-4.05	0.198	-0.802	0.105
9	19443	1.00	0.881	-0.0990	-0.0990	-0.0774
10	6.52×10^{-7}	1.00	0	0	0	0
11	-18259	-1.01×10^{5}	0.00779	-0.00698	-0.00698	-0.00673
12	53755	4.91×10^{4}	0.00222	-0.00182	-0.00182	-0.00171
13	1184	522	0.0164	-9.17×10^{-4}	-9.17×10^{-4}	-5.12×10^{-4}
14	52570	69.3	0.00352	-0.00313	-0.00313	-0.00302
15	1.95×10^{-3}	58.7	0.00650	-0.00577	-0.00577	-0.00559
16	17156	378	0.00946	-0.00349	-0.00349	-0.00322
17	6.97×10^{-2}	1.00	-7.73×10^{-4}	6.88×10^{-4}	6.88×10^{-4}	6.83×10^{-4}
18	-35414	-4.84×10^{3}	0.00411	-0.00438	-0.00438	-0.00422
19	-35414	-42.0	-0.0105	9.02×10^{-4}	9.02×10^{-4}	6.59×10^{-4}

3.3. Adding H_2O to the feed

It is clear from the DRCs in Table 6 that adding more water to reverse the net direction of steps (18) and (19), so that they go forward in net, should make the selectivity and rate to 1-BuOH go up. Table 7 shows the results of adding the maximum amount of water possible, its saturation vapor pressure, or 1 bar at this temperature of 373 K. Now step (11) has a major positive contribution to 1-BuOH production, rather than going in reverse to consume it, as in Table 6. This dramatically increases the selectivity for 1-butanol from 2.2% up to 70%, and the TOF to 1-butanol increases 30-fold over the low-water-pressure conditions of Table 6. Moreover, O_2 was consumed in making only 85% of the oxygen in products, with the remainder coming from the added H_2O. At the lower water pressure in Table 6, and in Tables 2-4, 100% of this oxygen came from O_2. This lower O_2 consumption could represent a cost and energy savings beyond that from the dramatically increased selectivity and TOF. The surface has a

Faraday Discussions Accepted Manuscript

relatively high coverage of adsorbed butanol at these conditions, ~0.25 ML. The OH* coverage increased 6-fold, from 0.0125 ML to 0.0734 ML.

Table 7. Steady state turnover frequencies (TOFs), ratio of forward TOF to net TOF, and degrees of rate control (X) obtained by solving the microkinetic model using the reactions listed in Tables 1 and 5. In this case, 101 kPa of H_2O was included in the feed, otherwise the conditions were the same as in Tables 2-4 and 6.

Rxn #	TOF (molecule site^{-1} s^{-1})	Forward TOF/ Net TOF	$X_{butanol}$	$X_{butanal}$	$X_{butene\ oxide}$	X_{butane}
1	21444	5.75×10^{4}	-2.16×10^{-5}	-5.99×10^{-5}	-5.97×10^{-5}	6.52×10^{-5}
2	21444	1.00	0.293	1.21	1.21	0.568
3	4.04×10^{-4}	1.00	0.00188	0.00568	0.00569	0.00308
4	50247	1.52	0.385	-0.502	-0.502	0.120
5	3.42×10^{-7}	1.00	4.01×10^{-4}	1.22×10^{-3}	1.22×10^{-3}	6.91×10^{-4}
6	1.34×10^{-7}	1.00	0	0	0	0
7	5.55×10^{-4}	1.00	0.00157	0.00477	1.00	0.00256
8	14887	1.00	-0.298	0.519	-0.481	-0.054
9	5553	1.00	-0.00852	-0.0826	-0.0826	-0.0306
10	3.42×10^{-7}	1.00	0	0	0	0
11	29707	1.37×10^{5}	0.00123	0.00372	0.00372	0.00197
12	50247	3.64×10^{4}	0.00200	0.00599	0.00599	0.00321
13	35260	51.2	0.0153	0.00264	0.00264	0.0116
14	14987	66.8	0.00213	0.00644	0.00644	0.00344
15	5.55×10^{-4}	41.0	-3.68×10^{-4}	-0.00112	-0.00112	-5.09×10^{-4}
16	22347	167	-0.00104	-0.00561	-0.00561	-0.00237
17	4.00×10^{-2}	1.00	4.67×10^{-4}	0.00142	0.00142	7.70×10^{-4}
18	7360	1.06×10^{6}	0.00116	0.00353	0.00353	0.00190
19	7360	7.01×10^{4}	8.30×10^{-4}	0.00250	0.00250	0.00137

Table 8 shows the corresponding DRCs and coverages of the adsorbed intermediates.

Faraday Discussions Accepted Manuscript

Table 8. Coverages and degrees of rate control for surface intermediates under the conditions of Table 7.

Intermediate	θ (ML)	$X_{butanol}$	$X_{butanal}$	$X_{butene\ oxide}$	X_{butane}
O*	6.45×10^{-4}	-9.60×10^{-5}	-0.000291	-0.000291	-9.13×10^{-5}
O_2*	0.0864	-0.0652	-0.198	-0.198	-0.105
C_4H_{10}*	0.015	-0.00987	-0.0299	-0.0299	-0.0157
C_4H_9*	2.03×10^{-10}	0	0	0	0
OH*	0.0734	-0.0539	-0.163	-0.163	-0.0865
C_4H_9O*	0.0102	-0.00856	-0.0260	-0.0260	-0.0137
H*	0.000830	0.00253	0.00767	0.00767	0.00411
C_4H_8Oep*	2.79×10^{-13}	0.00231	0.00701	0.00701	0.00380
C_4H_8Oal*	0.00844	-0.00636	-0.0193	-0.0193	-0.0102
C_4H_9OH*	0.245	-0.184	-0.558	-0.558	-0.296
H_2O*	0.0785	-0.060	-0.181	-0.181	-0.096
*	0.483	-	-	-	-

3.4. Increasing the butane pressure

It is clear from Table 7 that step (4) offers an opportunity to further improve the selectivity to 1–BuOH over butanal, since its DRC is +0.4 for 1-BuOH but -0.5 for butanal. Modifying the catalyst to decrease its activation barrier would lead to improved selectivity. A far simpler method to increase the rate of step (4) is to increase the butane coverage, since butane* is its reactant but adsorbed butane does not participate in any other kinetically relevant steps. To achieve this, we increased the partial pressure of butane up to its saturation value at 373 K, i.e., 1580 kPa, and recalculated the rates and DRCs at the same reaction conditions as in Tables 7-8. Indeed, the selectivity increased to 100%! The results are shown in Tables 9-10.The TOF to butanol also increased slightly, and the fraction of the oxygen in products that comes from O_2 decreased by 34%, to 51%, another major improvement. This addition of butane increased the butane coverage from 0.01 ML to 0.37 ML and correspondingly decreased the fraction of empty sites from 47% to 32%, which resulted in a similar relative decreased in the butanol coverage (from 0.25 ML to o.18 ML). The coverage of OH* decreased 8-fold, to 0.01 ML.

Faraday Discussions Accepted Manuscript

Table 9. Steady state turnover frequencies (TOFs), ratio of forward TOF to net TOF, and degrees of rate control (X) for elementary steps obtained by solving the microkinetic model using the reactions listed in Tables 1 and 5. In this case, 101 kPa of H_2O was included in the feed, and butane was fed at its saturation vapor pressure of 1580 kPa. All other conditions are the same as in Tables 6-8.

Rxn #	TOF (molecule site^{-1} s^{-1})	Forward TOF/ Net TOF	$X_{butanol}$	$X_{butanal}$	$X_{butene\ oxide}$	X_{butane}
1	9718	8.54×10^{4}	-0.00121	-0.00227	-0.00226	-0.00219
2	9718	1.00	0.753	1.89	1.89	0.753
3	6.82×10^{-3}	1.00	0.00870	0.0163	0.0163	0.00766
4	38332	1.06	0.0618	-1.34	-1.34	0.0580
5	1.81×10^{-7}	1.00	0.00542	0.0102	0.0102	0.00438
6	7.11×10^{-8}	1.00	0	0	0	0
7	1.51×10^{-6}	1.00	0.00628	0.0118	1.01	0.00602
8	41	1.00	0.000552	1.00	0.00110	0
9	456	1.00	-0.00946	-0.0237	-0.0237	-0.0131
10	1.81×10^{-7}	1.00	0.00224	0.00419	0.00420	0.00164
11	37835	1.65×10^{3}	0.0125	0.0228	0.0228	0.0109
12	38332	1.20×10^{6}	0.00259	0.00486	0.00486	0.00109
13	38292	34.2	-0.00877	-0.0478	-0.0478	-0.00985
14	41	6.41×10^{3}	0.000865	0.00162	0.00162	-0.00219
15	1.51×10^{-6}	27.9	0.00456	0.00854	0.00854	0.00274
16	18938	80.2	-0.00153	-0.00334	-0.00334	-0.00383
17	5.39×10^{-4}	1.00	-0.00987	-0.0185	-0.0185	-0.0120
18	18897	2.79×10^{5}	4.40×10^{-5}	7.86×10^{-5}	8.05×10^{-5}	-0.00219
19	18897	38.8	0.00196	0.00228	0.00229	0.00109

Table 10. Coverages and degrees of rate control for surface intermediates under the conditions of Table 9.

Intermediate	θ (ML)	$X_{butanol}$	$X_{butanal}$	$X_{butene\ oxide}$	X_{butane}
O*	1.36×10^{-5}	0.00270	0.00506	0.00506	0.00055
O_2*	0.0582	-0.0918	-0.172	-0.172	-0.0941
C_4H_{10}*	0.374	-0.577	-1.08	-1.08	-0.578
C_4H_9*	9.04×10^{-10}	0.00401	0.00752	0.00752	0.00274
OH*	0.00874	-0.0213	-0.0400	-0.0400	-0.0235
C_4H_9O*	0.00131	-0.00680	-0.0127	-0.0127	-0.00985
H*	0.000530	0.00783	0.0147	0.0147	0.00711
C_4H_8Oep*	0	0.00609	0.0114	0.0114	0.00602
C_4H_8Oal*	0.00220	-0.00449	-0.00842	-0.00842	-0.00547
C_4H_9OH*	0.177	-0.276	-0.517	-0.517	-0.277
H_2O*	0.0528	-0.0844	-0.158	-0.158	-0.0854
*	0.325	-	-	-	-

Faraday Discussions Accepted Manuscript

4. Conclusions

An $Ag_3Pd(111)$ surface decorated with a 2-atom-thick ring of (immobile) helium atoms which creates an artificial pore of similar size was used to model the sterically-constrained access to metal sites offered by a MOF-encapsulated PdAg nanoparticle catalyst. Using energies and kinetic parameters derived from DFT, a microkinetic model was developed to predict reaction rates and selectivities of this model catalyst for the regio-selective oxidation of n-butane to 1-butanol with O_2. The degrees of rate control of all species (adsorbed intermediates and transition states) were analysed to determine the rate controlling species and provide ideas for improvement. This revealed that the rate of production of adsorbed OH, required in the step to make adsorbed butanol, was dominated by the dehydrogenation of butoxy to make butanal plus OH. This severely limits selectivity to near 50%. This suggested that water should be added to the feed to make more OH, which indeed increased the rate to butanol and its selectivity increased dramatically, as summarized in Table 11. Moreover, far less O_2 was consumed per oxygen atom in the products. The degree of rate control for oxygen adatom addition to adsorbed butane to make butoxy plus H was positive for making 1-BuOH but negative for butanal, suggesting to increase the butane pressure. This indeed increased the selectivity to 1-BuOH dramatically, increased its rate and dramatically reduced O_2 consumption (Table 11).

Table 11. Summary of how changes in the reaction model and reaction conditions were used to markedly improve the butanol production rate, selectivity toward butanol, and amount of O in the products from O_2 (rather than H_2O). In all cases, the conditions were: T = 373 K, $P_{O2,0}$ = 21.3 kPa, $P_{C4H9OH,0} = P_{C4H8O,0} = P_{H2,0}$ = 0.01 kPa. Reaction steps (1)-(19) were all included except where noted. $P_{C4H10,0}$ = 2.0 kPa

Conditions	TOF to butanol (molecule site^{-1} s^{-1})	Butanol selectivity	O from O_2 / (Total O in product)
$P_{H2O,0}$ = 0, $P_{C4H10,0}$ = 42.6 kPa steps (18)-(19) excluded	31600	58%	100%
$P_{H2O,0}$ = 1.5 kPa, $P_{C4H10,0}$ = 42.6 kPa	923	2%	100%
$P_{H2O,0}$ = 101 kPa, $P_{C4H10,0}$ = 42.6 kPa	35200	70%	85%
$P_{H2O,0}$ = 101 kPa, $P_{C4H10,0}$ = 1580 kPa	38300	100%	51%

Faraday Discussions Accepted Manuscript

5. Acknowledgements

This research was funded in part by the DOE EFRC Inorganometallic Catalyst Design Center (grant number DE-SC0012702, Principal Investigator Laura Gagliardi at the University of Minnesota), the National Science Foundation (Award DMR-1334928), and the Clemson University Calhoun Honors College. Simulations were performed on the Palmetto Supercomputer Cluster, which is maintained by the Cyberinfrastructure Technology Integration Group at Clemson University.

6. References

1. G. Lu, S. Li, Z. Guo, O. K. Farha, B. G. Hauser, X. Qi, Y. Wang, X. Wang, S. Han, X. Liu, J. S. DuChene, H. Zhang, Q. Zhang, X. Chen, J. Ma, S. C. J. Loo, W. D. Wei, Y. Yang, J. T. Hupp and F. Huo, *Nature Chem.*, 2012, **4**, 310-316.
2. S. L. James, *Chem. Soc. Rev.*, 2003, **32**, 276-288.
3. H. Furukawa, K. E. Cordova, M. O'Keeffe and O. M. Yaghi, *Science*, 2013, **341**.
4. H. Li, M. Eddaoudi, M. O'Keeffe and O. M. Yaghi, *Nature*, 1999, **402**, 276-279.
5. C. J. Stephenson, J. T. Hupp and O. K. Farha, *Inorg. Chem. Front.*, 2015.
6. D. A. Gomez-Gualdron, S. T. Dix, R. B. Getman and R. Q. Snurr, *Phys. Chem. Chem. Phys.*, 2015, **17**, 27596-27608.
7. S. T. Dix, D. A. Gomez-Gualdron and R. B. Getman, *Surface Science*, under review.
8. C. Stegelmann, A. Andreasen and C. T. Campbell, *Journal of the American Chemical Society*, 2009, **131**, 8077-8082.
9. C. A. Wolcott, A. J. Medford, F. Studt and C. T. Campbell, *J. Catalysis*, 2015, **330**, 197-207.
10. G. Kresse and J. Furthmuller, *Computational Materials Science*, 1996, **6**, 15-50.
11. G. Kresse and J. Furthmuller, *Physical Review B*, 1996, **54**, 11169-11186.
12. J. P. Perdew, K. Burke and M. Ernzerhof, *Physical Review Letters*, 1996, **77**, 3865-3868.
13. J. P. Perdew, K. Burke and M. Ernzerhof, *Phys. Rev. Lett.*, 1997, **78**, 1396.
14. P. E. Blochl, *Phys. Rev. B*, 1994, **50**, 17953-17979.
15. G. Kresse and D. Joubert, *Physical Review B*, 1999, **59**, 1758–1775.
16. S. Grimme, *J. Comput. Chem.*, 2006, **27**, 1787-1799.
17. G. Henkelman and H. Jonsson, *J. Chem. Phys.*, 2000, **113**, 9901-9904.
18. G. Henkelman and H. Jonsson, *J. Chem. Phys.*, 2000, **113**, 9978-9985.
19. G. Henkelman and H. Jonsson, *J. Chem. Phys.*, 1999, **111**, 7010-7022.
20. M. Borbach, W. Stenzel, H. Conrad and A. M. Bradshaw, *Surface Science*, 1997, **377**, 796-801.
21. W. Lew, M. C. Crowe, E. Karp, O. Lytken, J. A. Farmer, L. Arnadottir, C. Schoenbaum and C. T. Campbell, *Journal of Physical Chemistry C*, 2011, **115**, 11586-11594.

Faraday Discussions Accepted Manuscript